


Dynamical phase transition and scaling in the chiral clock Potts chainXue-Jia Yu ^{*}*Department of Physics, Fuzhou University, Fuzhou, Fujian 350116, China
and Fujian Key Laboratory of Quantum Information and Quantum Optics, College of Physics and
Information Engineering, Fuzhou University, Fuzhou, Fujian 350108, China*

(Received 6 September 2023; accepted 28 November 2023; published 18 December 2023)

Based on time-dependent variational-principle algorithms, we investigate the dynamical critical behavior of quantum three-state Potts chains with chiral interactions. Using the Loschmidt echo, dynamical order parameter, and entanglement entropy as an indicator, we show that as the chiral interaction θ increases, the first critical time t_1^* shifts towards lower values, indicating a chirality-related dynamical phase transition. Moreover, we perform dynamical scaling for the Loschmidt echo and obtain the critical exponent ν at the nonconformal critical point. The results show that as the chiral interaction θ increases, the correlation-length exponent ν decreases, which is similar to the long-range interaction case. Finally, we give a simple physical argument to understand the above numerical results. This work provides a useful reference for further research on many-body physics out of equilibrium with chiral interaction.

DOI: [10.1103/PhysRevA.108.062215](https://doi.org/10.1103/PhysRevA.108.062215)**I. INTRODUCTION**

Understanding exotic phases and phase transitions in many-body systems is a fundamental challenge in the field of condensed-matter and statistical physics [1–4]. While extensive studies have been focused on equilibrium phase transitions [5–9], less attention has been paid to the behavior of quantum many-body systems out of equilibrium [10,11]. The dynamical quantum phase transition (DQPT) [12–18] is a type of nonequilibrium phase transition that occurs at critical times t^* during real-time evolution, characterized by nonanalyticities of the rate function after a sudden quench of the system [17]. Analogous to equilibrium phase transitions that arise from singularities in parameter space, the DQPT originates from singularities in time [12,16,17]. Recently, there has been a surge of interest in the study of the DQPT, including investigations into critical behavior [15,19–35], order parameters [36–41], spontaneously broken symmetries [14], and experimental realizations across a variety of platforms [42–49].

On the one hand, quantum phase transitions were previously investigated and found to possess relativistic and conformal invariance, allowing for significant analytical progress [50–52]. However, there has long been debate surrounding the commensurate-incommensurate phase transition [53–63] regarding whether there is an intermediate floating phase between the commensurate-incommensurate phases studied in the 1980s or, if it is a continuous phase transition, what universality class this phase transition belongs to. This debate has to be revisited due to the potential of a neutral long-range interacting Rydberg-atom array confined in optical tweezers to serve as a tunable platform for observing a variety of quantum phenomena [64,65]. Similarly, the \mathbb{Z}_3 clock model with chiral interaction also exhibits such nonconformal chiral transition [53,66–71]. An intriguing question within the chiral

clock model therefore arises: What is the relationship between the chiral and long-range interactions in quantum critical behavior [53,56,72]?

On the other hand, previous studies on the DQPT across different quantum critical points were carried out in many systems, such as the symmetry-breaking critical point [12,14], topological phase transitions [36,73,74], an exotic deconfined quantum critical point [41], and even a non-Hermitian critical point [21,75,76]. Although the link between the DQPT and many physical observables has been established [16–18], a thorough understanding of this transition still calls for more studies. To the best of our knowledge, whether the DQPT can occur in a system after a quench across a nonconformal critical point and its dynamical scaling behavior have been less studied so far; therefore, it is very worthwhile to study and demonstrate the possible existence of a DQPT in the system with a nonconformal critical point.

To answer the two questions above, in this work, we explore the dynamical behavior of a \mathbb{Z}_3 -symmetric quantum spin chain with chiral interaction. Our investigation utilizes a time-dependent variational-principle (TDVP) simulation [77–80] to examine the effect of chiral interaction; we show that the introduction of chiral interaction can advance the first critical time of the DQPT. Furthermore, our analysis of the Loschmidt echo reveals that the correlation-length critical exponent decreases as the chiral interaction increases, which agrees with previous studies of long-range interacting Rydberg-atom arrays. The results imply chiral interaction and long-range interaction have similar effects on quantum critical behavior.

This paper is organized as follows: Sec. II presents the lattice model of the quantum Potts chain with chiral interaction, the numerical method used, and the physical quantities that display a DQPT. In Sec. III, we provide benchmark results for DQPT in nearest-neighbor quantum Potts chains and chirality-related dynamical phase transitions. Section IV presents the dynamical scaling for the Loschmidt echo to

^{*}xuejiayu@fzu.edu.cn

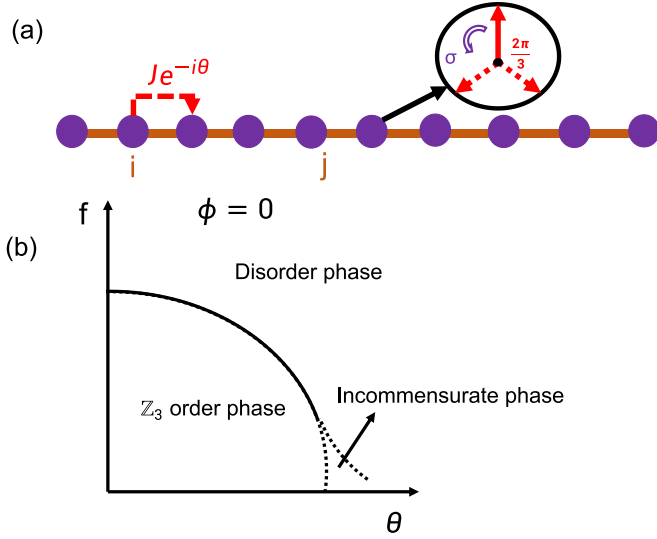


FIG. 1. (a) Schematic chiral interaction θ and ϕ and (b) ground phase diagram with respect to the chiral interaction θ and external transverse field f of the quantum chiral clock Potts chain with $\phi = 0$ [53,71]. With a nonzero chiral interaction phase ($\theta \neq 0$), the effective interaction can induce incommensurate floating phases with respect to the periodicity of the underlying lattice, and the transition between the \mathbb{Z}_3 order phase and disorder phase belongs to the nonconformal chiral universality class.

obtain critical behavior in the chiral transition, as well as a simple physical explanation for our numerical observations. Finally, our conclusion is presented in Sec. V. Appendixes provide additional data for our numerical calculations.

II. MODEL AND METHOD

The system we study is a quantum chiral Potts chain of L spins (see Fig. 1), described by the following Hamiltonian [53,66,71,81–85]:

$$H_{\text{CCM}} = -J \sum_{j=1}^N \sigma_j^\dagger \sigma_{j+1} e^{-i\theta} - f \sum_j \tau_j^\dagger e^{-i\phi} + \text{H.c.}, \quad (1)$$

where ϕ and θ define two types of chiral interactions (temporal and spatial, respectively). The main text focuses on the $\phi = 0$ case, where time-reversal and spatial-parity symmetry are both preserved but the chirality is still present as a purely spatial one (for the temporal case see Appendix C). J is the interaction strength, and f represents the external transverse field. The Hilbert space is $(\mathbb{C}^3)^{\otimes N}$. τ dictates the direction of the watch hand, and σ rotates the watch hand clockwise through a discrete angle $2\pi/3$, as shown in Fig. 1(a). σ and τ satisfy $\sigma_i^3 = I$, $\tau_i^3 = I$, and $\sigma_i \tau_j = \omega \delta_{ij} \tau_j \sigma_i$, where $\omega = e^{2\pi i/3}$. A global \mathbb{Z}_3 transformation represented by $G = \prod_i \tau_i$ makes the Hamiltonian invariant. The operators are defined by

$$\sigma = \begin{pmatrix} 0 & 1 & 0 \\ 0 & 0 & 1 \\ 1 & 0 & 0 \end{pmatrix}, \quad \tau = \begin{pmatrix} 1 & 0 & 0 \\ 0 & \omega & 0 \\ 0 & 0 & \omega^2 \end{pmatrix}. \quad (2)$$

The introduction of chiral interaction has a significant impact on the phase diagram [as shown in Fig. 1(b)] and has

been extensively studied in the literature [53,71]. Specifically, in the absence of chiral interaction ($\theta = \phi = 0$), the model reduces to the standard nearest-neighbor quantum three-state Potts chain. In this case, for $f \ll J$, the system is in an ordered phase that breaks the \mathbb{Z}_3 symmetry, while for $f \gg J$, it is in a disordered paramagnetic phase. Fradkin-Kadanoff's transformation demonstrates that the system exhibits a continuous phase transition from the Potts-ordered topological phase to a trivial disordered phase, with a correlation-length exponent of $\nu = 5/6$ [66,67,70,71]. In the presence of a nonzero chiral interaction, the effective interaction can be induced incommensurate floating phases relative to the lattice periodicity, and the transition between gapped states belongs to a nonconformal chiral universality class. Furthermore, the model is known to be integrable for a two-parameter family of couplings along the line $f \cos(3\phi) = J \cos(3\theta)$ and is exactly solvable.

To exhibit a DQPT, we first consider the Loschmidt amplitude (return amplitude), which was been introduced by Heyl *et al.* [12],

$$\mathcal{L}(t) = \langle \psi_i | \psi(t) \rangle = \langle \psi_i | e^{-iH_f t} | \psi_i \rangle, \quad (3)$$

where $|\psi_i\rangle$ denotes the ground state that pertains to the Hamiltonian before quench H_i (or, more generally, an arbitrary initial state) and evolves under quenched Hamiltonian H_f in time. The structure of the Loschmidt amplitude resembles the boundary partition function defined in statistical mechanics, except the time-evolution operator makes it a complex quantity instead of real. This analogy suggests the introduction of the effective free energy (return rate)

$$r(t) = -\frac{1}{N} \lim_{N \rightarrow \infty} \ln |\mathcal{L}|^2; \quad (4)$$

similar to the equilibrium statistical physics, where phase transitions are identified by singularities in the free energy at certain values of the control parameter, the DQPT is characterized by nonanalytic cusps in the return rate $r(t)$ at the time t^* . However, a specific nonequilibrium protocol, such as a quantum quench, can be employed to observe a DQPT by driving the system out of equilibrium. In the case of a quantum quench, the initial state is prepared as the ground state of an initial Hamiltonian H_0 , and then the control parameter of the Hamiltonian is suddenly switched to a different value, leading to the final Hamiltonian H_f .

The relationship between the dynamical order parameter and the DQPT is an intriguing topic that has recently attracted considerable interest. The dynamical order parameter accurately characterizes the behavior of the Loschmidt echo; specifically, the periodic behavior exhibited by the dynamical order parameters should be the same as the period of the Loschmidt echo [41]. This definition does not necessitate conformity with the characteristics of order parameters in equilibrium quantum phase transitions. To explore this relation in the nonconformal quantum critical point, we introduce a dynamical order parameter defined as $Q(t) = \frac{1}{L} \langle \psi(t) | \sum_j (\tau_j + \tau_j^\dagger) | \psi(t) \rangle$.

Additionally, the relationship between the DQPT and entanglement structures has also been investigated. The DQPT may correspond to regions of rapid growth or peaks in entanglement entropy [44,86]. To further probe the DQPT,

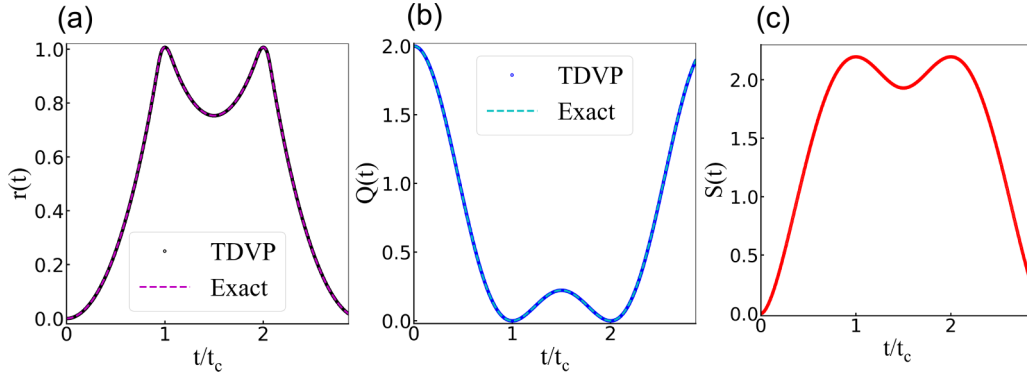


FIG. 2. Time evolution of (a) the return rate, (b) dynamical order parameter, and (c) entanglement entropy. Purple and cyan dashed lines represent exact analytic results from the transfer matrix. All the plots correspond to quenches with $f_0/J = \infty$ (PM) $\rightarrow f_1/J = 0.0$ (Potts FM), $\theta = \phi = 0$, and $N = 30$. $t_c = 2\pi/9$ is the first critical time for the three-state Potts chain as the system size N tends to ∞ .

we define the entanglement entropy as $S(t) = -\text{Tr}(\rho_A \ln \rho_A)$, where $\rho_A = \text{Tr}_B |\psi(t)\rangle\langle\psi(t)|$ is the reduced density matrix about half chain A : $1, 2, \dots, N/2$ (for B , $N/2 + 1, \dots, N$).

Except for specific integrable lines, the quantum chiral clock Potts chain does not have exact solutions. In the parameter region of interest, we employ a state-of-the-art, time-dependent density-matrix renormalization-group (DMRG) method (more precisely, the TDVP method) [77–80] based on matrix product states (MPSs), which is a powerful numerical method for one-dimensional strongly correlated many-body systems. We set the bond dimension to 60, ensuring good convergence of the dynamical physical quantities (see Appendix G) by requiring relative energy errors to be less than 10^{-5} . The time step during the evolution is set to $dt = 0.001$ (ensuring good convergence; see Appendix A). To minimize edge effects, we impose periodic boundary conditions and use $J = 1$ as the energy unit. It is worth emphasizing that, in our cases, the finite-size TDVP algorithm is more efficient than the infinite density matrix renormalization group (iDMRG) algorithm for computing other physical quantities, such as entanglement entropy.

III. DYNAMICAL PHASE TRANSITION

As a benchmark, we first study the DQPT of the nearest-neighbor quantum three-state Potts chain ($\theta = \phi = 0$) [87–89]. More precisely, we study the time evolution of the return rate after sudden quenches between the paramagnetic (PM) and Potts ferromagnetic (Potts FM) phases.

We first consider a special limit in which the return rate can be obtained analytically, starting from the perfect PM phase ($f_0 = \infty$) and quenched to the classical Potts FM phase ($f_1 = 0$). The initial state is given by

$$|\psi_0\rangle = \frac{1}{3^{N/2}} \prod_i (|A\rangle_i + |B\rangle_i + |C\rangle_i), \quad (5)$$

where $|A\rangle_i$, $|B\rangle_i$, and $|C\rangle_i$ are three degenerate Potts FM ground states. Since the final Hamiltonian is purely classical, the return amplitude can be written in the simple form

$$\mathcal{L}(t) = \text{tr} M^N, \quad M = \begin{pmatrix} e^{2iJt}/3 & e^{-iJt}/3 & e^{-iJt}/3 \\ e^{-iJt}/3 & e^{2iJt}/3 & e^{-iJt}/3 \\ e^{-iJt}/3 & e^{-iJt}/3 & e^{2iJt}/3 \end{pmatrix}, \quad (6)$$

where periodic boundary conditions on a chain with N lattice sites have been considered. The eigenvalues of the transfer matrix M are given by

$$\lambda_1 = \frac{e^{-iJt}}{3} (e^{3iJt} + 2), \quad \lambda_2 = \lambda_3 = \frac{e^{-iJt}}{3} (e^{3iJt} - 1), \quad (7)$$

and we obtain the return amplitude $\mathcal{L}(t) = \lambda_1(t)^N + 2\lambda_2(t)^N$, which yields the return rate

$$l(t) = -\frac{1}{N} \ln |(9\cos^2\tilde{t} + \sin^2\tilde{t})^N + 4^{N+1}\sin^2\tilde{t} + 2(2i)^N(3\cos\tilde{t} + isin\tilde{t})^N \sin^N\tilde{t} + 2(2i)^N(-3\cos\tilde{t} + isin\tilde{t})^N \sin^N\tilde{t}| + 2\ln 3, \quad (8)$$

where $\tilde{t} = 3Jt/2$. The return rate is periodic, $l(t) = l(t + 2\pi/3J)$, $l(0) = 0$, and shows nonanalytic behavior at the critical times $Jt^* = 2\pi/9 + 2\pi n/3$, $n \in \mathbb{N}_0$, as shown in Fig. 2.

A. Warm-up: Quantum Potts chains

In this section, we numerically investigate the DQPT after quenches from the PM phase to the Potts FM phase. The quench protocol is implemented by suddenly switching the ratio between the transverse field f and ferromagnetic interaction J from its initial value f_0/J to its final value f_1/J . We start from the PM state, which is obtained from the initial Hamiltonian H_0 with $f_0 = 1.0$, $J = 0.0$, and $f_0/J = \infty$, quenched to a final state with parameters $f_1 = 0.0$, $J = 1.0$, and $f_1/J = 0.0$, located in the Potts FM order phase. The general relation between the DQPT and the underlying equilibrium quantum critical point is unclear, but as argued in previous works [16,17], the DQPT usually occurs when the quenching process is ramped through an equilibrium critical point. Indeed, as shown in Fig. 2(a), the return rate exhibits nonanalytical behavior with respect to time, implying the DQPT occurs (see Appendix A for the finite-size scaling), and the time evolution behavior of the return rate is the same as that for the iDMRG results [87]. Moreover, to explore the relationship between the return rate and the zeros of a dynamical order parameter, we also calculate the dynamical order parameter. During the time evolution, the dynamical order parameter exhibits periodic changes with time, with its

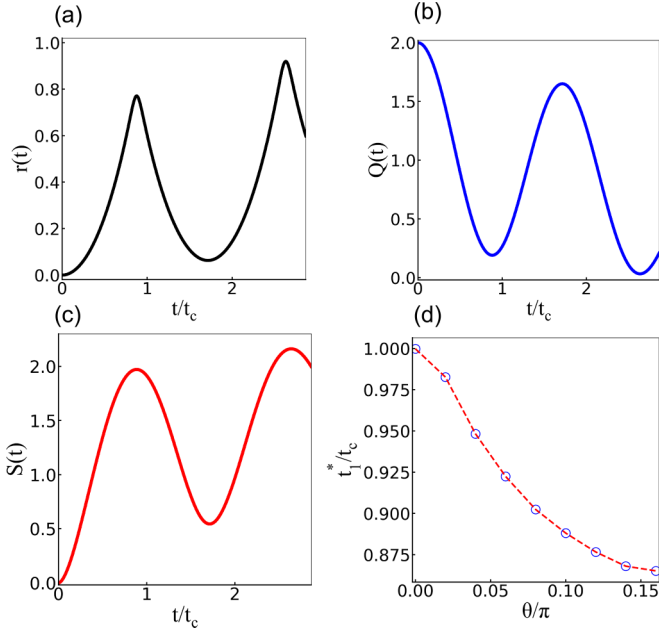


FIG. 3. Time evolution of (a) the return rate, (b) dynamical order parameter, and (c) entanglement entropy. (d) The first critical time as a function of the spatial chiral interaction θ . The plots correspond to quenches with $f_0/J = \infty$ (PM) $\rightarrow f_1/J = 0.0$ (Potts FM), $\theta = 0.12\pi$, $\phi = 0$, and $N = 30$.

valleys corresponding to the peaks in the return rate, as shown in Fig. 2(b). Our numerical observation is fully consistent with previous studies [87].

Moreover, we can explore the entanglement structures and possible connections to the above observations. The entanglement entropy is an efficient physical quantity to uncover entanglement structures of the model. To be more precise, the half-chain entanglement entropy is a singular value of the Schmidt decomposition across a bond and is easily accessed through the finite-size DMRG calculation. In Fig. 2(c), sudden changes in the entanglement entropy are seen in the vicinity of the several critical times, which is similar to the dynamical behavior of the return rate. The reason for this currently remains unclear but suggests some deeper relationship between the entanglement structure and DQPT. It is important to note that while the dynamical order parameters and entanglement entropy exhibit peaks, these peaks do not increase with system size (up to $N = 30$; see Appendix A). This suggests that the dynamical order parameter or entanglement entropy alone cannot be used as an indicator of whether a DQPT has occurred at this time. However, it is noteworthy that the period of change in the dynamical order parameter and entanglement entropy coincides with the period of the DQPT.

B. Chirality-related dynamical phase transition

We note that the asymmetry in the Hamiltonian has important consequences: The spatial chirality ($\theta \neq 0$) induces incommensurate floating phases with respect to the periodicity of the underlying lattice. To study whether chirality will affect the DQPT of the system, we numerically investigate the quantum chiral Potts chain with $\theta = 0.12\pi$, quenched from

the PM to the Potts FM phase. On the one hand, we start from the PM state, which is obtained from the initial Hamiltonian H_0 with $f_0 = 1.0$, $J = 0.0$, and $f_0/J = \infty$, quenched to a final state with parameters $f_1 = 0.0$, $J = 1.0$, and $f_1/J = 0.0$, located in Potts FM order phase. As shown in Fig. 3(a), we find that the return rate exhibits a series of nonanalytic behaviors with time, implying that the introduction of chirality is stable for observing a DQPT. On the other hand, we also calculate the dynamical order parameter and entanglement entropy, as shown in Figs. 3(b) and 3(c), and find that the valley (peak) of the dynamical order parameter (entanglement entropy) corresponds to the peak of the return rate, demonstrating that they have the same periodicity of the DQPT. Moreover, as shown in Fig. 3(d), we found that the first critical time t_1^* for the DQPT decreases with the increase of the chiral interaction (see Appendix B for the calculation of the DQPT of another chiral interaction). This means that the increase in chiral interaction will make it easier for a DQPT to occur; we call this the “chirality-related dynamical phase transition.” This adjustment allows for the observation of DQPTs in a shorter time, thereby reducing the experimental detection complexity associated with these transitions. In Sec. IV C, we will give a simple physical argument to explain this phenomenon. Finally, we also calculate the DQPT from the Potts FM to the PM phase with the temporal chiral interaction ϕ . The results are shown in Appendix C.

IV. DYNAMICAL SCALING FOR A CHIRAL CLOCK POTTS CHAIN

A. Fidelity susceptibility and the quantum critical point

The system undergoes a continuous phase transition from an ordered to a disordered phase when tuning the external field f , after which the structure of the ground-state wave function changes significantly. The quantum ground-state fidelity $F(f, f + \delta f)$ is defined as the wave-function overlap of two neighboring ground states with respect to an external field f , and its value is almost zero near the quantum critical point f_c^* . In practice, the more convenient quantity to characterize quantum phase transitions is the fidelity susceptibility, defined by the leading term of the fidelity [56,90–94],

$$\chi_F(f) = \lim_{\delta f \rightarrow 0} \frac{2[1 - F(f, f + \delta f)]}{(\delta f)^2}. \quad (9)$$

The fidelity susceptibility is a geometric property of quantum states in the realm of quantum information that offers a distinct advantage in that it requires no *a priori* knowledge of order parameters or symmetry breaking. It has been applied to detect a wide range of quantum phase transitions [41,55,95–98] induced by a sudden change in the structure of the wave function. Experimental detection of quantum phase transitions using fidelity susceptibility can be achieved via neutron scattering or angle-resolved photoemission spectroscopy techniques [90]. Here we employ the fidelity susceptibility [99] to identify the critical point in the quantum Potts chain with chiral interaction and perform dynamical scaling in the obtained quantum critical point.

Figure 4(a) illustrates the scaling behavior of fidelity susceptibility per site $\chi_N = \chi_F/N$ as a function of system size N for $\theta = 0.12\pi$ in the quantum Potts chain with chiral

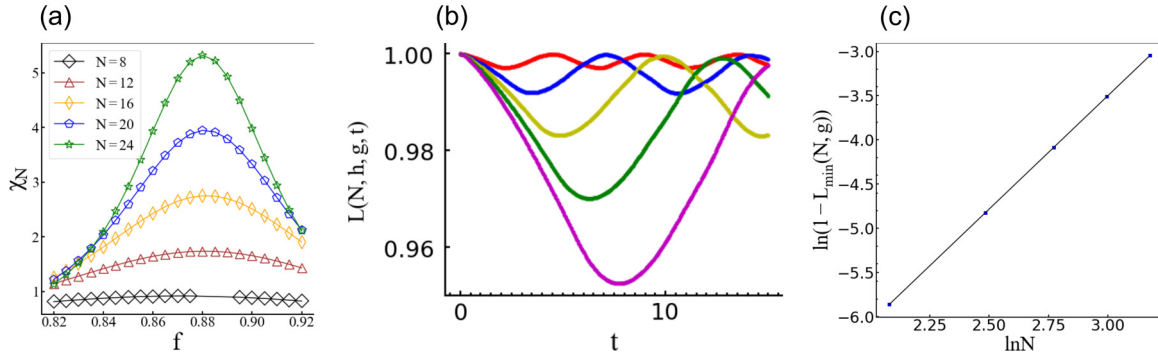


FIG. 4. (a) Fidelity susceptibility per site χ_N of the quantum Potts chain with chiral interaction for $\theta = 0.12\pi$ and $N = 8, 12, 16, 20, 24$ sites as a function of external transverse field f ; symbols denote finite-size DMRG results. (b) The Loschmidt echo $L(N, f, g, t)$ at the peak position f of χ_N in (a) with $g = 0.01$ as a function of time t for lattice sizes $N = 8$ (red), 12 (blue), 16 (yellow), 20 (green), and 24 (purple; from top to bottom along the first minimum). (c) Finite-size scaling of $1 - L_{\min}(N, g)$ obtained from (b) as a function of lattice sizes N , where the black squares are numerical values and the black solid line denotes the fitting curve. The correlation-length critical exponent $\nu = 0.780 \pm 0.001$ is obtained from the fitting curve.

interaction. As the system size increases from $N = 8$ to 24, we observe that the peak position of the fidelity susceptibility curve gradually approaches the exact critical point f_c^* . Our results indicate that the peak of the fidelity susceptibility converges at $N = 24$ (see Appendix A for the finite-size effect of the DQPT), providing an effective means of obtaining the quantum critical point. (See Appendix E for details on the calculation of the fidelity susceptibility for another chiral interaction.)

B. Dynamical scaling law for the Loschmidt echo

As a next step, we aim to examine the dynamical property of the system following a small quench and carry out dynamical scaling of the Loschmidt echo to obtain critical exponents in the nonconformal chiral universality class. Recent studies [20] demonstrated that the decay of the Loschmidt echo can be enhanced by the equilibrium quantum criticality. The first minimum of the Loschmidt echo at t_1^* can be scaled as

$$1 - L_{\min}(N, g) \propto g^2 N^{2/\nu} \quad (10)$$

at the equilibrium chiral transition point. Here ν is the correlation-length exponent, and g is a small constant step, defined as $g = f_1 - f_0$, where f_0 and f_1 are the external field before and after quench protocols. The exact definition of the first minimum of the Loschmidt echo is $L_{\min}(N, g) = \min_t |\langle \psi_0(f_0) | e^{-iH_f t} | \psi_0(f_0) \rangle|^2$. The dynamical scaling law in Eq. (10) that governs the critically enhanced decay behavior of the Loschmidt echo with respect to N can be utilized to extract the correlation-length exponent ν . In order to perform the scaling law in Eq. (10) for the Loschmidt echo $L_{\min}(N, g)$, it should be computed at or close to the equilibrium critical point f_c^* , which is obtained from fidelity susceptibility.

To this end, we first obtain the ground state ψ_0 from Eq. (1) at the external field f_0 and then compute the Loschmidt echo from Eq. (3) by quenching the chiral clock Potts chain from the initial f_0 to the final f_1 with a small constant step $g = 0.01$. The time-evolved wave function $\psi(t)$ is obtained from the TDVP with a step $dt = 0.02$ under periodic boundary conditions, where we set $J = 1$ during the numerical simulations. We perform numerical simulations upon a quench

with the TDVP from this critical point f_0 to $f_1 = f_0 + g$ for $N = 8, 12, 16, 20, 24$ sites. The results of the Loschmidt echo $L(N, h, g, t)$ for $\theta = 0.12\pi$ shown in Fig. 4(b) exhibit a decay and revival dynamics. The first minimum of the Loschmidt echoes $L_{\min}(N, g)$ is plotted in Fig. 4(c) with respect to the lattice size N . According to the scaling law in Eq. (10), we obtain the correlation-length exponent $\nu = 0.780 \pm 0.001$ for a nonconformal chiral transition. Details on the dynamical scaling of the Loschmidt echo for another chiral interaction can be found in Appendix D, and the results for all θ are summarized in Table I. The results show that the correlation-length exponent ν decreases with increasing chiral interaction θ , which is consistent with previous studies [53,55,56]. Moreover, we want to remark that when $\theta = \pi$, the model is simplified to a quantum antiferromagnetic Potts chain. Under this condition, the Kosterlitz–Thouless transition (KT)-like phase transition from the massive trivial phase to the massless phase will occur. The critical point is located at $f/J \approx 0.2$ [100,101] (due to the symmetry of the three-state chiral Potts model, $\theta = \theta + \pi/3$, $\theta = \pi$ is equivalent to $\pi/3$; therefore, the phase transition from a massive trivial phase to a massless incommensurate phase occurs [71]). In the context of the KT transition, the correlation length exhibits divergence characterized by $\xi \propto \exp(Cf^{-\nu}) \propto \exp(C/\sqrt{f})$, where the

TABLE I. Critical exponents of the Potts chain with different chiral interactions θ . Critical exponents are obtained by dynamical scaling for the Loschmidt echoes.

θ	ν
0.0π	0.838(4)
0.02π	0.832(4)
0.04π	0.829(3)
0.06π	0.824(3)
0.08π	0.813(1)
0.10π	0.7978(5)
0.12π	0.780(1)
0.14π	0.754(2)
0.16π	0.724(3)

“correlation-length exponent” ν is known to be 0.5 [58,102]. However, comprehensive understanding of DQPTs resulting from a quench across a KT transition, as well as the associated dynamical scaling laws, remains an open issue. We defer this intriguing topic to future work.

C. Discussion

In this section, we present a brief discussion on the physical reason for the emergence of the chirality-related dynamical phase transition. First, the introduction of the spatial chiral interaction θ can be considered an equivalent of introducing power-law long-range interactions. To be precise, when the spatial chiral interaction is increased (i.e., larger θ), the interaction becomes longer range. Recent studies [53] on Rydberg-atom arrays demonstrated that the van der Waals long-range interaction has an effect on the critical behavior similar to the chiral interaction. In particular, the longer the power-law interaction is, the smaller the critical exponent of the correlation length ν is, which is consistent with the results obtained by dynamical scaling (see Table I). This is because the long-range interactions enhance the inequivalence between the two types of domain walls, leading to a faster deviation from the Potts exponent [55].

On the other hand, previous reports [103–111] studied the dynamical phase transitions in the transverse field Ising model with power-law long-range interactions $1/r^\alpha$. According to Fig. 1 of Ref. [103], when $\alpha < 2.0$ (where the physics is essentially analogous to that of a short-range Ising model for large α), a smaller power-law long-range interaction exponent α implies a stronger long-range interaction and, consequently, effectively enhances chirality, as discussed previously. This results in a lower critical transverse field required for the appearance of kinks in the Loschmidt echo under identical quenching conditions, which means that the DQPT will occur earlier; that is, the first critical time will decrease (advance).

By combining the two aspects above, we provide a simple physical explanation for chirality-related dynamical phase transition: The effect of the spatial chiral interaction is akin to that of long-range interaction, and the introduction of long-range interaction enhances the propensity for a DQPT in the system. Therefore, spatial chiral interaction can effectively advance the dynamical phase transition. Finally, we observe that the inclusion of temporal chiral interaction leads to different results (see Appendix C), which merits further detailed investigation in the future.

V. CONCLUSION AND OUTLOOK

To summarize, we investigated the quench dynamics in the \mathbb{Z}_3 -symmetric spin chain with chiral interaction. To establish a baseline, we first considered the standard nearest-neighbor quantum three-state Potts chain and derived analytical results of the Loschmidt echo for the quench from the PM to the Potts FM phase. Our results showed that the Loschmidt echo, dynamical order parameter, and entanglement entropy exhibit DQPT signatures. We then investigated more general cases with a chiral interaction θ using TDVP algorithms. The results revealed that the introduction of the chiral interaction will advance the critical time of the DQPT, which we refer to as

a chirality-related dynamical phase transition. Additionally, we performed dynamical scaling for the Loschmidt echo and obtained the correlation-length critical exponent ν under different chiral interactions. The numerical results indicated that as the chiral interaction increases, the correlation-length exponent ν decreases, which has an effect similar to long-range interaction. Finally, we provided a simple physical argument to understand the chirality-related dynamical phase transition.

Future work may explore the physical reason for the dynamical phase transition due to temporal chiral interaction and investigate the fate of quench dynamics in two-dimensional systems with different types of quantum critical points. Our work may provide insights into many-body physics out of equilibrium with chiral interaction.

ACKNOWLEDGMENTS

X.-J.Y. thanks G. Sun, S. Yang, and C.-X. Li for helpful discussions. Numerical simulations were carried out with the ITENSOR package [112]. X.-J. Yu acknowledges support from the start-up Grant No. 511317 of Fuzhou University.

APPENDIX A: FINITE SIZE AND RIME STEP EFFECT OF THE DQPT

In this Appendix, we investigate the effect of the finite system sizes on the extraction of the dynamical properties, namely, the associated return rate $r(t)$, dynamical order parameter $Q(t)$, and entanglement entropy $S(t)$. To this end, we perform TDVP calculations for different system sizes N from 9 to 30 sites with periodic boundary conditions and consider a quench originating in the PM phase with $\phi = \theta = 0$, $f_0 = 1.0$, $J = 0.0$, and $f_0/J = \infty$ and, subsequently, a quench to the Potts FM phase with $f_1 = 0.0$, $J = 1.0$, and $f_1/J = 0.0$, as shown in Fig. 5. It is clear that the return rate $r(t)$ of the largest four system sizes is quite good, with only a slight deviation of the smallest two sizes, which indicates that the system size $N = 30$ is sufficient to detect the DQPT, and we notice that the dynamical order parameter and entanglement entropy do not appear as a shape peak but exhibit the time evolution of the same period as the return rate. This does not change with system size. Therefore, we can expect that Figs. 1–4 in the main text reliably represent the results in the thermodynamic limit. In addition, we also calculate the return rate under different time steps $dt = 0.01, 0.005, 0.0025$, and 0.001 , and the results show that the result of $dt = 0.001$ basically converges, as shown in Fig. 5(d).

APPENDIX B: EVOLUTION OF THE DYNAMICAL PHASE TRANSITION WITH THE CHIRAL INTERACTION

In this Appendix, we provide additional data to show the dynamical phase transition evolves with the chiral interaction.

Figure 6 shows the return rate $r(t)$ of the Potts chain with chiral interaction for $\theta = 0.02\pi, 0.04\pi, 0.06\pi, 0.08\pi, 0.1\pi, 0.14\pi$, and 0.16π and $N = 30$ sites as a function of time t . We found that no matter the return rate, dynamical order parameter, and entanglement entropy, the time when the kink (that is, the DQPT) appears for the first time decreases

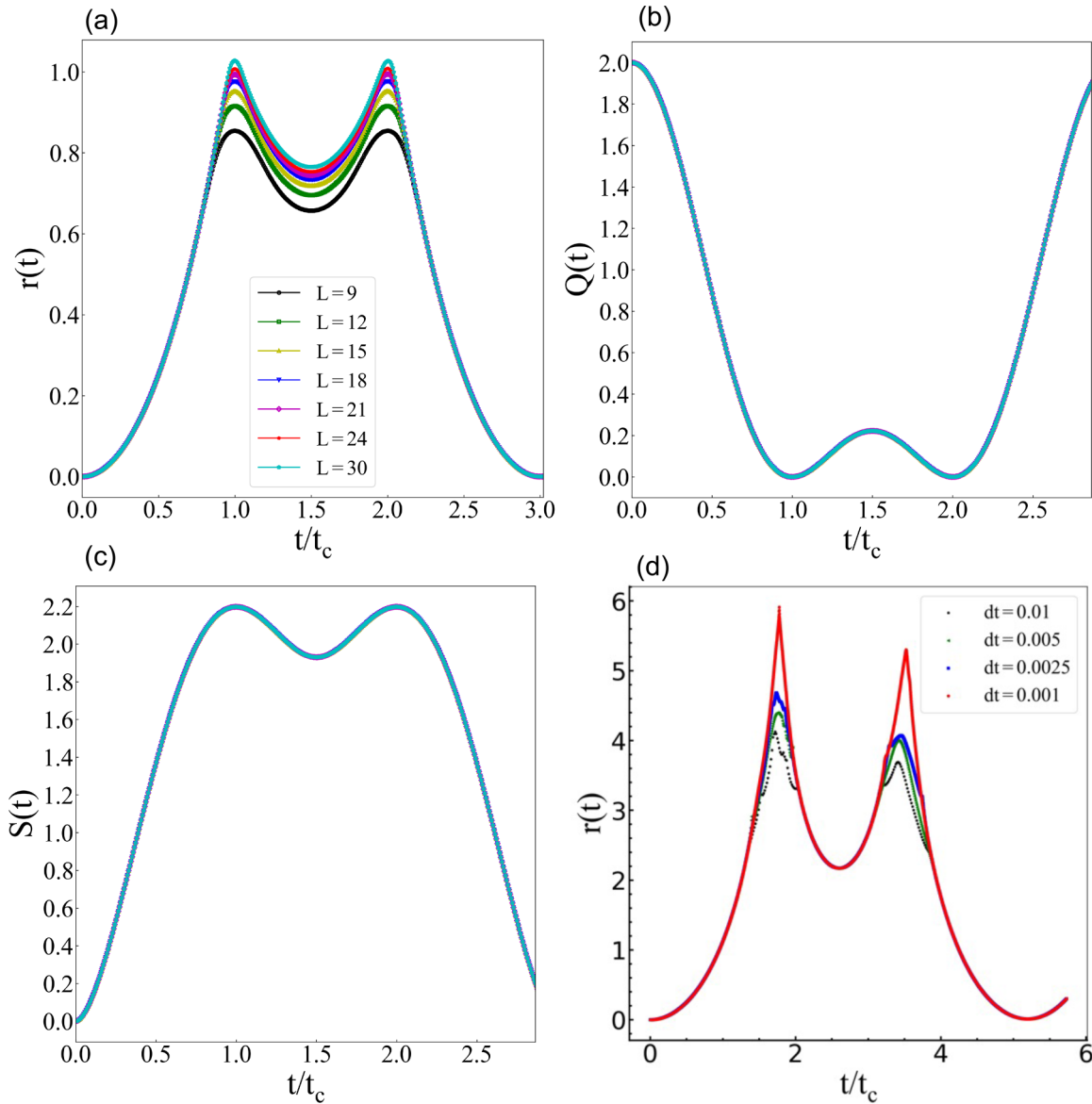


FIG. 5. (a) The return rate as a function of time for system size N from 9 to 30 sites across the critical point. (b) Dynamical order parameter and (c) entanglement entropy. It is clear that the return rate $r(t)$ of the largest four system sizes is quite good, with only a slight deviation of the smallest two sizes. (a)–(c) correspond to the PM state and quench to the final Potts FM state. (d) The return rate as a function of time for different time steps dt from 0.01 to 0.001 across the critical point for $\phi = 0.12\pi$, $\theta = 0.0$, and $N = 30$. (d) corresponds to the quenches from the Potts FM state and quench to the final PM phase.

with the increase of θ , which is a chirality-related dynamical phase transition in the main text.

APPENDIX C: QUENCH FROM POTTS TO PM WITH TEMPORAL CHIRAL INTERACTION

We briefly discuss the DQPT of the Potts model with temporal chiral interaction. To this end, we start from the Potts FM state ($f_0 = 0.0, J = 1.0, f_0/J = 0.0$) and quench to the PM state ($f_1 = 1.0, J = 0.0, f_1/J = \infty$) with the temporal chiral interaction phase ϕ . The return rate of the Potts chain with chiral interaction for $\phi = 0.02\pi, 0.04\pi, 0.06\pi, 0.08\pi, 0.1\pi, 0.14\pi$, and 0.16π and $N = 30$ sites as a function of time t exhibits singular behavior,

as shown in Fig. 7. We give the first critical time t_1^* as a function of the temporal chiral interaction phase ϕ for $\phi = 0.12\pi$ and $N = 30$ combined with the return rate in Fig. 8. The results show that t_1^* increases with the increase of ϕ , in contrast to the spatial chiral interaction case.

APPENDIX D: DYNAMICAL SCALING FOR OTHER CHIRAL INTERACTION PHASES

In this Appendix, we provide additional data to show dynamical scaling for other chiral interaction phases.

Figures 9(a)–9(h) show the dynamical scaling for $1 - L_{\min}(N, g)$ in the Potts chain with chiral interaction for $\theta = 0.0\pi, \theta = 0.02\pi, \theta = 0.04\pi, \theta = 0.06\pi, \theta = 0.08\pi$,

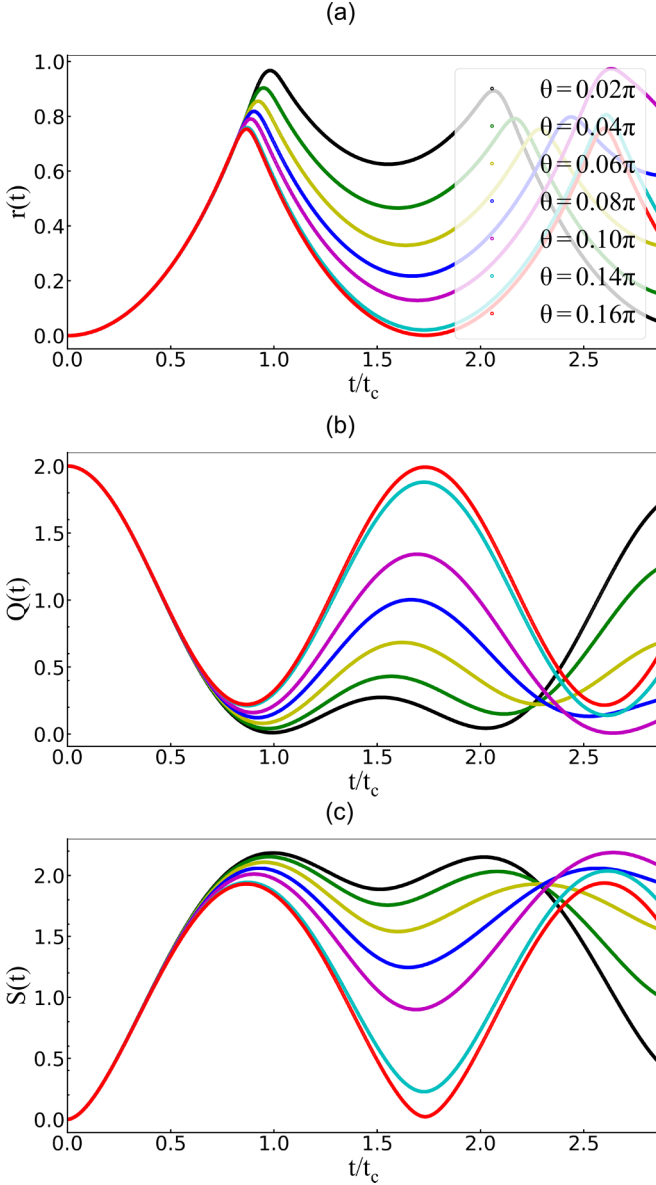


FIG. 6. Time evolution of (a) the return rate, (b) dynamical order parameter, and (c) entanglement entropy of the quantum Potts chain with spatial chiral interaction ($\phi = 0.0$) for $\theta = 0.02\pi, 0.04\pi, 0.06\pi, 0.08\pi, 0.1\pi, 0.14\pi$, and 0.16π and $N = 30$. All the plots correspond to quenches with $f_0/J = \infty$ (PM) \rightarrow $f_1/J = 0.0$ (Potts FM).

$\theta = 0.1\pi$, $\theta = 0.14\pi$, and $\theta = 0.16\pi$ and $N = 8, 12, 16, 20, 24$ sites as a function of lattice size N , respectively. The extrapolated correlation-length exponents are summarized in Table I; we find that with the enhancement of chiral interaction θ , the correlation-length exponent ν of the system gradually decreases, which is consistent with the effect of long-range interaction.

APPENDIX E: FIDELITY SUSCEPTIBILITY FOR OTHER CHIRAL INTERACTION PHASES

In this Appendix, we provide additional data to show the fidelity susceptibility for other chiral interaction phases.

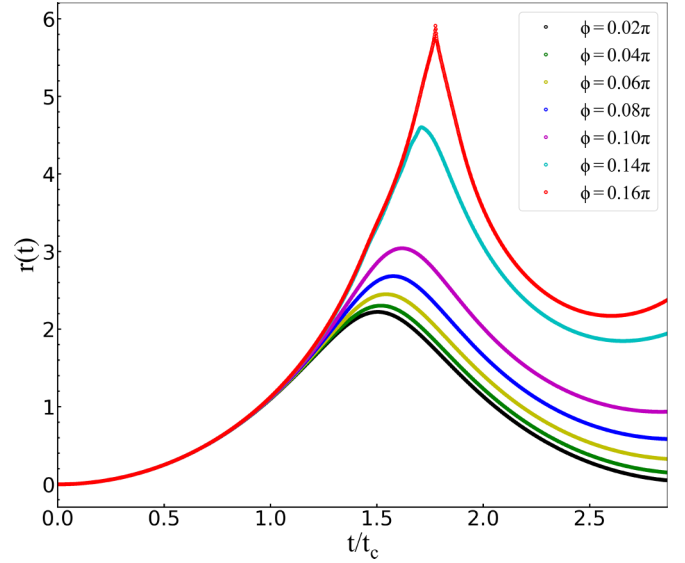


FIG. 7. Time evolution of the return rate of the quantum Potts chain with temporal chiral interaction ($\theta = 0.0$) for $\phi = 0.02\pi, 0.04\pi, 0.06\pi, 0.08\pi, 0.1\pi, 0.14\pi$, and 0.16π and $N = 30$. The plot corresponds to quenches with $f_0/J = 0.0$ (Potts FM) \rightarrow $f_1/J = \infty$ (PM).

Figures 10(a)–10(h) show the fidelity susceptibility per site $\chi_N = \chi_F/N$ of the Potts chain with chiral interaction for $\theta = 0.0\pi$, $\theta = 0.02\pi$, $\theta = 0.04\pi$, $\theta = 0.06\pi$, $\theta = 0.08\pi$, $\theta = 0.1\pi$, $\theta = 0.14\pi$, and $\theta = 0.16\pi$ and $N = 8, 12, 16, 20, 24$ sites as a function of the external transverse field f , respectively. We find that quantum critical points are shifted to lower values of f as chiral interaction increases.

APPENDIX F: LOSCHMIDT ECHO AT THE PEAK POSITION FOR OTHER CHIRAL INTERACTION PHASES

In this Appendix, we provide additional data to show the Loschmidt echo at the peak position for other chiral interaction phases.

Figures 11(a)–11(h) show the Loschmidt echo at the peak position of the Potts chain with chiral interaction for $\theta = 0.0\pi$, $\theta = 0.02\pi$, $\theta = 0.04\pi$, $\theta = 0.06\pi$, $\theta = 0.08\pi$,

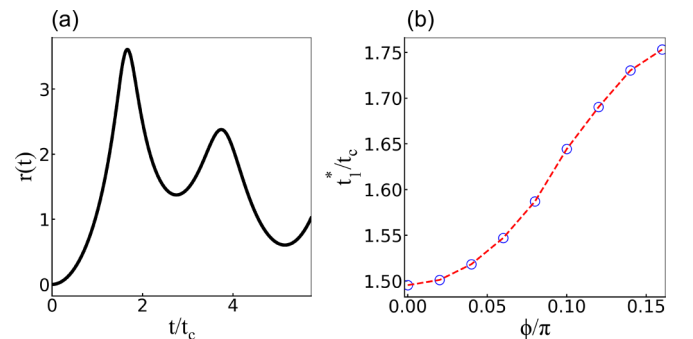


FIG. 8. (a) Time evolution of the return rate. The plot corresponds to quenches with $f_0/J = 0.0$ (Potts FM) \rightarrow $f_1/J = \infty$ (PM), $\theta = 0.0$, $\phi = 0.12\pi$, and $N = 30$. (b) The first critical time is a function of the temporal chiral interaction phase ϕ .

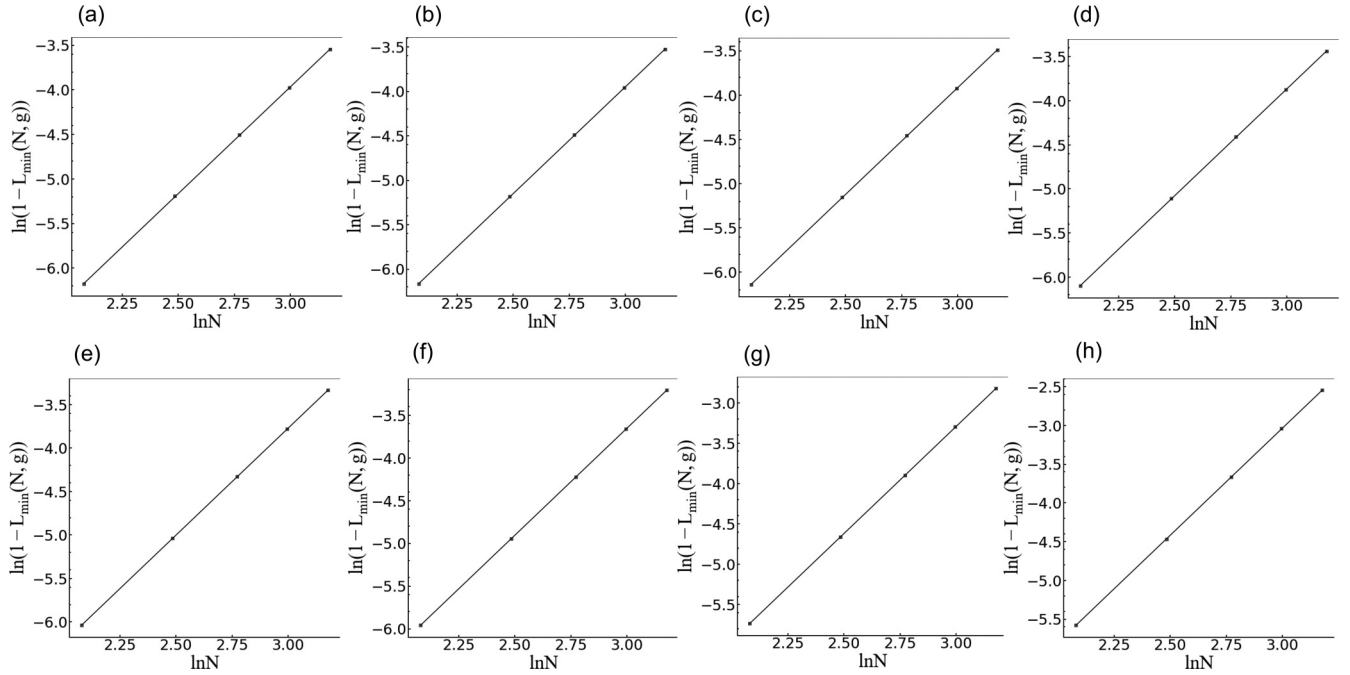


FIG. 9. Finite-size scaling of $1 - L_{\min}(N, g)$ of the quantum Potts chain with spatial chiral interaction ($\phi = 0.0$) for (a) $\theta = 0.0\pi$, (b) $\theta = 0.02\pi$, (c) $\theta = 0.04\pi$, (d) $\theta = 0.06\pi$, (e) $\theta = 0.08\pi$, (f) $\theta = 0.1\pi$, (g) $\theta = 0.14\pi$, and (h) $\theta = 0.16\pi$ and $N = 8, 12, 16, 20, 24$ sites as a function of lattice size N ; symbols denote finite-size DMRG results.

$\theta = 0.1\pi$, $\theta = 0.14\pi$, and $\theta = 0.16\pi$ and $N = 8, 12, 16, 20, 24$ sites as a function of time t , respectively. We find that the time to the first appearance of the kink increases with increasing chiral interaction.

APPENDIX G: QUENCH FROM THE FM POTTS ORDER TO THE PM PHASE WITH SPATIAL CHIRAL INTERACTION AND BOND DIMENSION DEPENDENCE

In this Appendix, we conduct TDVP simulations across various chiral interaction strengths ($\theta = 0.0\pi, 0.2\pi$, and

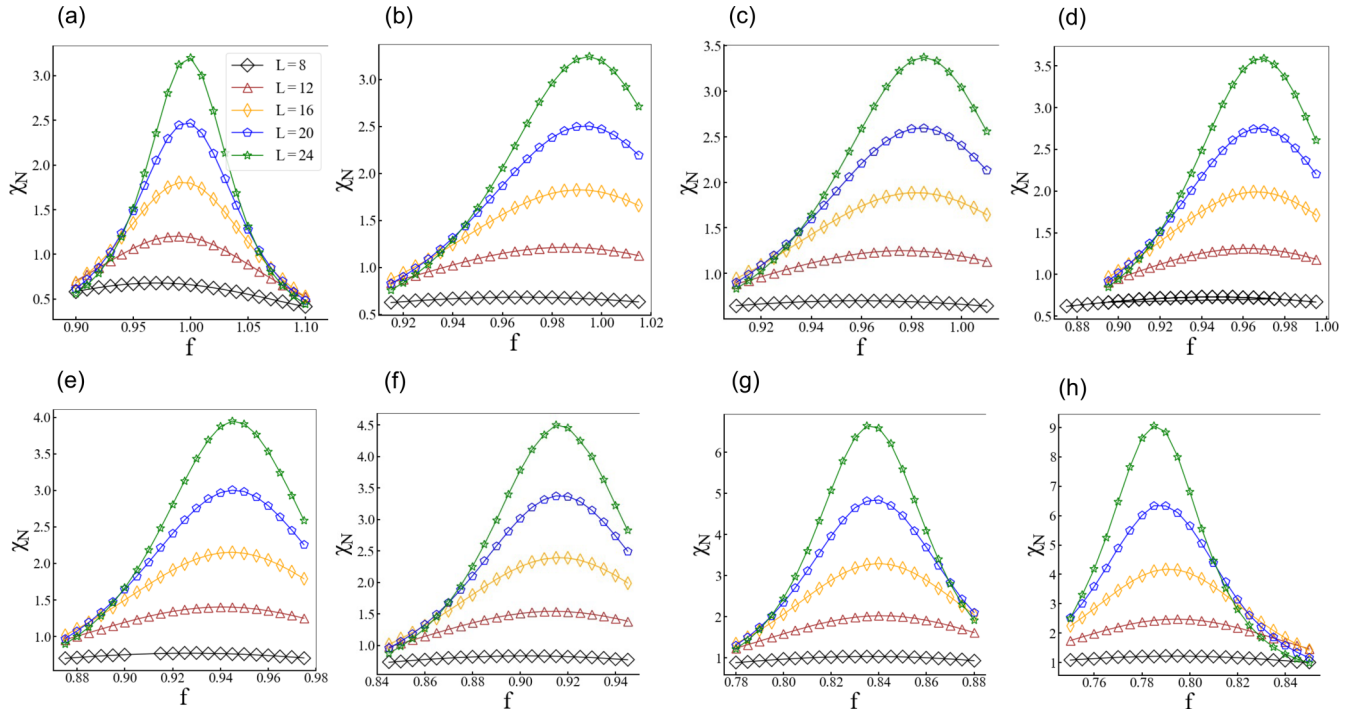


FIG. 10. Fidelity susceptibility per site χ_N of the quantum Potts chain with spatial chiral interaction ($\phi = 0.0$) for (a) $\theta = 0.0\pi$, (b) $\theta = 0.02\pi$, (c) $\theta = 0.04\pi$, (d) $\theta = 0.06\pi$, (e) $\theta = 0.08\pi$, (f) $\theta = 0.1\pi$, (g) $\theta = 0.14\pi$, and (h) $\theta = 0.16\pi$ and $N = 8, 12, 16, 20, 24$ sites as a function of external transverse field f ; symbols denote finite-size DMRG results.

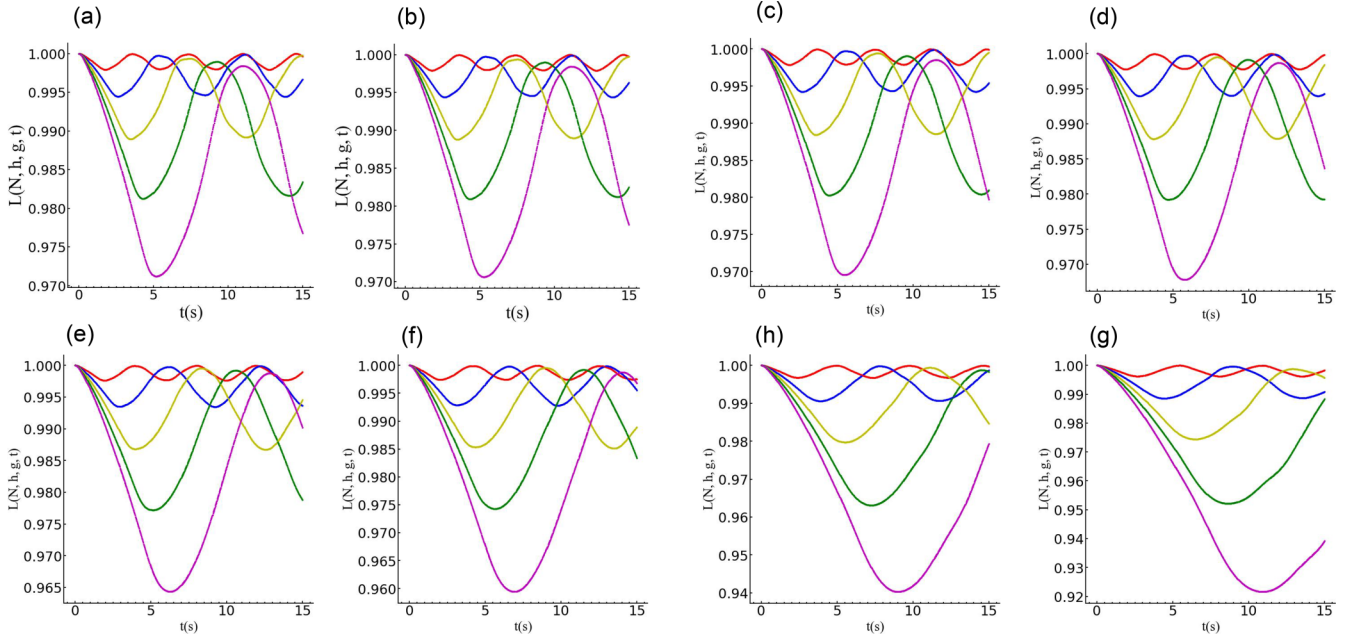


FIG. 11. The Loschmidt echo $L(N, f, g, t)$ at the peak position f of χ_L with $g = 0.01$ of the quantum Potts chain with spatial chiral interaction ($\phi = 0.0$) for (a) $\theta = 0.0\pi$, (b) $\theta = 0.02\pi$, (c) $\theta = 0.04\pi$, (d) $\theta = 0.06\pi$, (e) $\theta = 0.08\pi$, (f) $\theta = 0.1\pi$, (h) $\theta = 0.16\pi$, and (g) $\theta = 0.14\pi$ and $N = 8$ (red), 12 (blue), 16 (yellow), 20 (green), and 24 (purple) sites as a function of time t ; symbols denote finite-size TDVP results.

1.0π) while utilizing periodic boundary conditions. To be more precise, we consider a quench starting from the Potts FM phase with $\phi = 0$, $f_0 = 0.0$, $J = 1.0$, and $f_0/J = 0.0$, subsequently quenching to the PM phase with $f_1 = 1.0$, $J = 0.0$, and $f_1/J = \infty$, as depicted in Fig. 12(a). Notably, when $\theta = 0$, as previously established, there is no occurrence of the DQPT in this case [87]. As we introduce the chiral interaction, we observe a gradual smoothing of the peak value

of the return rate, and yet the system still does not undergo a DQPT.

Furthermore, we vary the MPS bond dimension χ to investigate its impact on the return rate, as the return rate is directly related to the observation of a DQPT, as shown in Fig. 12(b). The results reveal that the return rate converges when χ exceeds 32. Therefore, utilizing $\chi = 60$ in the main text for the dynamical calculations is sufficient to ensure result convergence.

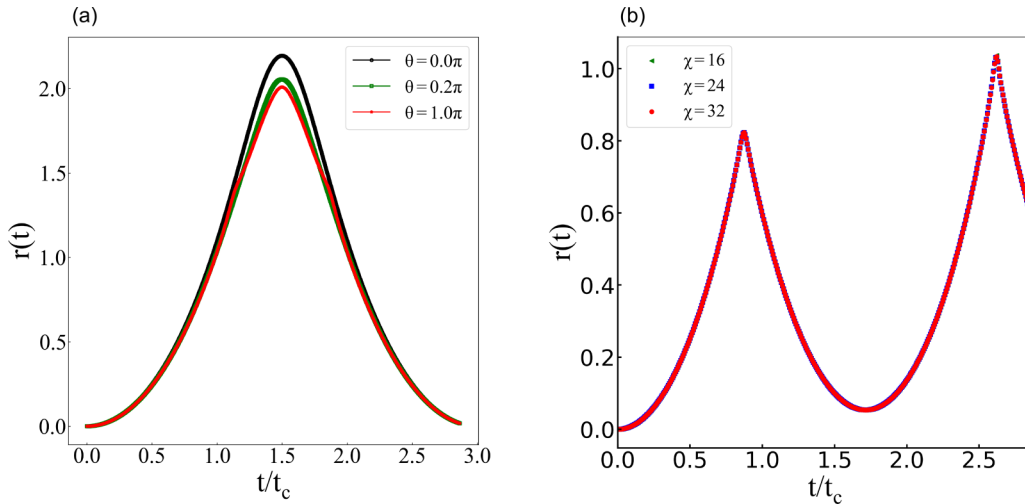


FIG. 12. The return rate as a function of time (a) for chiral interaction θ for 0.0π , 0.2π , and 1.0π and (b) for different bond dimensions $\chi = 16, 24, 32$ for $\theta = 0.12\pi$ across the critical point. Starting from the Potts FM phase and quenching to the final PM phase for $N = 30$.

- [1] S. Sachdev, *Quantum Phase Transitions* (Cambridge University Press, Cambridge, 2011).
- [2] S. Sachdev, *Quantum Phases of Matter* (Cambridge University Press, Cambridge, 2023).
- [3] J. Cardy, *Scaling and Renormalization in Statistical Physics* (Cambridge University Press, Cambridge, 1996).
- [4] C. Xu, *Int. J. Mod. Phys. B* **26**, 1230007 (2012).
- [5] S. L. Sondhi, S. M. Girvin, J. P. Carini, and D. Shahar, *Rev. Mod. Phys.* **69**, 315 (1997).
- [6] M. E. Fisher and M. N. Barber, *Phys. Rev. Lett.* **28**, 1516 (1972).
- [7] M. E. Fisher, *Rev. Mod. Phys.* **46**, 597 (1974).
- [8] X.-J. Yu, P.-L. Zhao, S.-K. Jian, and Z. Pan, *Phys. Rev. B* **105**, 205140 (2022).
- [9] Z.-X. Guo, X.-J. Yu, X.-D. Hu, and Z. Li, *Phys. Rev. A* **105**, 053311 (2022).
- [10] G. Ódor, *Rev. Mod. Phys.* **76**, 663 (2004).
- [11] H. Weimer, A. Kshetrimayum, and R. Orús, *Rev. Mod. Phys.* **93**, 015008 (2021).
- [12] M. Heyl, A. Polkovnikov, and S. Kehrein, *Phys. Rev. Lett.* **110**, 135704 (2013).
- [13] M. Heyl, *Phys. Rev. Lett.* **115**, 140602 (2015).
- [14] S. A. Weidinger, M. Heyl, A. Silva, and M. Knap, *Phys. Rev. B* **96**, 134313 (2017).
- [15] J.-C. Tang, W.-L. You, M.-J. Hwang, and G. Sun, *Phys. Rev. B* **107**, 134303 (2023).
- [16] M. Heyl, *Europhys. Lett.* **125**, 26001 (2019).
- [17] M. Heyl, *Rep. Prog. Phys.* **81**, 054001 (2018).
- [18] A. A. Zvyagin, *Low Temp. Phys.* **42**, 971 (2016).
- [19] H. T. Quan, Z. Song, X. F. Liu, P. Zanardi, and C. P. Sun, *Phys. Rev. Lett.* **96**, 140604 (2006).
- [20] M.-J. Hwang, B.-B. Wei, S. F. Huelga, and M. B. Plenio, *arXiv:1904.09937*.
- [21] J.-C. Tang, S.-P. Kou, and G. Sun, *Europhys. Lett.* **137**, 40001 (2022).
- [22] C. Ding, *Phys. Rev. B* **102**, 060409(R) (2020).
- [23] Y.-T. Zou and C. Ding, *Phys. Rev. B* **108**, 014303 (2023).
- [24] J. Naji, R. Jafari, L. Zhou, and A. Langari, *Phys. Rev. B* **106**, 094314 (2022).
- [25] R. Jafari, A. Akbari, U. Mishra, and H. Johannesson, *Phys. Rev. B* **105**, 094311 (2022).
- [26] J. Naji, M. Jafari, R. Jafari, and A. Akbari, *Phys. Rev. A* **105**, 022220 (2022).
- [27] M. Sadrzadeh, R. Jafari, and A. Langari, *Phys. Rev. B* **103**, 144305 (2021).
- [28] S. Zamani, R. Jafari, and A. Langari, *Phys. Rev. B* **102**, 144306 (2020).
- [29] R. Jafari and A. Akbari, *Phys. Rev. A* **103**, 012204 (2021).
- [30] U. Mishra, R. Jafari, and A. Akbari, *J. Phys. A* **53**, 375301 (2020).
- [31] P. Urich, N. Defenu, R. Jafari, and J. C. Halimeh, *Phys. Rev. B* **101**, 245148 (2020).
- [32] R. Jafari, H. Johannesson, A. Langari, and M. A. Martin-Delgado, *Phys. Rev. B* **99**, 054302 (2019).
- [33] R. Jafari and H. Johannesson, *Phys. Rev. Lett.* **118**, 015701 (2017).
- [34] N. A. Khan, P. Wang, M. Jan, and G. Xianlong, *Sci. Rep.* **13**, 9470 (2023).
- [35] N. A. Khan, X. Wei, S. Cheng, M. Jan, and G. Xianlong, *Phys. Lett. A* **475**, 128880 (2023).
- [36] M. Heyl, *Phys. Rev. B* **95**, 060504(R) (2017).
- [37] Y.-P. Huang, D. Banerjee, and M. Heyl, *Phys. Rev. Lett.* **122**, 250401 (2019).
- [38] O. N. Kuliashov, A. A. Markov, and A. N. Rubtsov, *Phys. Rev. B* **107**, 094304 (2023).
- [39] R. Vosk and E. Altman, *Phys. Rev. Lett.* **112**, 217204 (2014).
- [40] I. Hagymási, C. Hubig, O. Legeza, and U. Schollwöck, *Phys. Rev. Lett.* **122**, 250601 (2019).
- [41] G. Sun and B.-B. Wei, *Phys. Rev. B* **102**, 094302 (2020).
- [42] T. Tian, H.-X. Yang, L.-Y. Qiu, H.-Y. Liang, Y.-B. Yang, Y. Xu, and L.-M. Duan, *Phys. Rev. Lett.* **124**, 043001 (2020).
- [43] X.-Y. Guo, C. Yang, Y. Zeng, Y. Peng, H.-K. Li, H. Deng, Y.-R. Jin, S. Chen, D. Zheng, and H. Fan, *Phys. Rev. Appl.* **11**, 044080 (2019).
- [44] P. Jurcevic, H. Shen, P. Hauke, C. Maier, T. Brydges, C. Hempel, B. P. Lanyon, M. Heyl, R. Blatt, and C. F. Roos, *Phys. Rev. Lett.* **119**, 080501 (2017).
- [45] N. Fläschner, D. Vogel, M. Tarnowski, B. Rem, D.-S. Lühmann, M. Heyl, J. Budich, L. Mathey, K. Sengstock, and C. Weitenberg, *Nat. Phys.* **14**, 265 (2018).
- [46] K. Wang, X. Qiu, L. Xiao, X. Zhan, Z. Bian, W. Yi, and P. Xue, *Phys. Rev. Lett.* **122**, 020501 (2019).
- [47] T. Tian, Y. Ke, L. Zhang, S. Lin, Z. Shi, P. Huang, C. Lee, and J. Du, *Phys. Rev. B* **100**, 024310 (2019).
- [48] X. Nie, B.-B. Wei, X. Chen, Z. Zhang, X. Zhao, C. Qiu, Y. Tian, Y. Ji, T. Xin, D. Lu, and J. Li, *Phys. Rev. Lett.* **124**, 250601 (2020).
- [49] L.-N. Wu, J. Nettersheim, J. Feß, A. Schnell, S. Burgardt, S. Hiebel, D. Adam, A. Eckardt, and A. Widera, *arXiv:2208.05164*.
- [50] P. Francesco, P. Mathieu, and D. Sénéchal, *Conformal Field Theory* (Springer Science & Business Media, New York, 2012).
- [51] P. Ginsparg, *arXiv:hep-th/9108028*.
- [52] X.-J. Yu, R.-Z. Huang, H.-H. Song, L. Xu, C. Ding, and L. Zhang, *Phys. Rev. Lett.* **129**, 210601 (2022).
- [53] R. Samajdar, S. Choi, H. Pichler, M. D. Lukin, and S. Sachdev, *Phys. Rev. A* **98**, 023614 (2018).
- [54] S. Whitsitt, R. Samajdar, and S. Sachdev, *Phys. Rev. B* **98**, 205118 (2018).
- [55] X.-J. Yu, S. Yang, J.-B. Xu, and L. Xu, *Phys. Rev. B* **106**, 165124 (2022).
- [56] X.-J. Yu, C. Ding, and L. Xu, *Phys. Rev. E* **107**, 054122 (2023).
- [57] Y. Cheng and C. Li, *Phys. Rev. B* **107**, 094302 (2023).
- [58] N. Chepiga and F. Mila, *Phys. Rev. Lett.* **122**, 017205 (2019).
- [59] I. A. Maccira, N. Chepiga, and F. Mila, *Phys. Rev. Res.* **4**, 043102 (2022).
- [60] S. Nyckees and F. Mila, *Phys. Rev. Res.* **4**, 013093 (2022).
- [61] N. Chepiga and F. Mila, *Phys. Rev. Res.* **3**, 023049 (2021).
- [62] S. Nyckees, J. Colbois, and F. Mila, *Nucl. Phys. B* **965**, 115365 (2021).
- [63] N. Chepiga and F. Mila, *Nat. Commun.* **12**, 414 (2021).
- [64] A. Keesling, A. Omran, H. Levine, H. Bernien, H. Pichler, S. Choi, R. Samajdar, S. Schwartz, P. Silvi, S. Sachdev, P. Zoller, M. Endres, M. Greiner, V. Vuletić, and M. D. Lukin, *Nature (London)* **568**, 207 (2019).
- [65] M. Serbyn, D. A. Abanin, and Z. Papić, *Nat. Phys.* **17**, 675 (2021).
- [66] P. Fendley, *J. Stat. Mech.* (2012) P11020.
- [67] P. Fendley, *J. Phys. A* **47**, 075001 (2014).

- [68] R. S. K. Mong, D. J. Clarke, J. Alicea, N. H. Lindner, and P. Fendley, *J. Phys. A* **47**, 452001 (2014).
- [69] A. S. Jermyn, R. S. K. Mong, J. Alicea, and P. Fendley, *Phys. Rev. B* **90**, 165106 (2014).
- [70] J. Alicea and P. Fendley, *Annu. Rev. Condens. Matter Phys.* **7**, 119 (2016).
- [71] Y. Zhuang, H. J. Changlani, N. M. Tubman, and T. L. Hughes, *Phys. Rev. B* **92**, 035154 (2015).
- [72] R.-Z. Huang and S. Yin, *Phys. Rev. B* **99**, 184104 (2019).
- [73] J. C. Budich and M. Heyl, *Phys. Rev. B* **93**, 085416 (2016).
- [74] C. Yang, L. Li, and S. Chen, *Phys. Rev. B* **97**, 060304(R) (2018).
- [75] L. Zhou, Q.-H. Wang, H. Wang, and J. Gong, *Phys. Rev. A* **98**, 022129 (2018).
- [76] T. Hayata, Y. Hidaka, and A. Yamamoto, *Prog. Theor. Exp. Phys.* **2023**, 023102 (2023).
- [77] U. Schollwöck, *Ann. Phys. (NY)* **326**, 96 (2011).
- [78] U. Schollwöck, *Rev. Mod. Phys.* **77**, 259 (2005).
- [79] S. R. White and A. E. Feiguin, *Phys. Rev. Lett.* **93**, 076401 (2004).
- [80] M. Yang and S. R. White, *Phys. Rev. B* **102**, 094315 (2020).
- [81] S. Ostlund, *Phys. Rev. B* **24**, 398 (1981).
- [82] D. A. Huse, *Phys. Rev. B* **24**, 5180 (1981).
- [83] J. H. H. Perk, *J. Phys. A: Math. Theor.* **49**, 153001 (2016).
- [84] R. Baxter, J. Perk, and H. Au-Yang, *Phys. Lett. A* **128**, 138 (1988).
- [85] H. Au-Yang, B. M. McCoy, J. H. Perk, S. Tang, and M.-L. Yan, *Phys. Lett. A* **123**, 219 (1987).
- [86] M. Schmitt and M. Heyl, *SciPost Phys.* **4**, 013 (2018).
- [87] C. Karrasch and D. Schuricht, *Phys. Rev. B* **95**, 075143 (2017).
- [88] Y. Wu, [arXiv:1908.04476](https://arxiv.org/abs/1908.04476).
- [89] Y. Wu, *Phys. Rev. B* **101**, 014305 (2020).
- [90] S.-J. Gu and W. C. Yu, *Europhys. Lett.* **108**, 20002 (2014).
- [91] S.-J. Gu, *Int. J. Mod. Phys. B* **24**, 4371 (2010).
- [92] S.-J. Gu, *Phys. Rev. E* **79**, 061125 (2009).
- [93] S.-J. Gu and H.-Q. Lin, *Europhys. Lett.* **87**, 10003 (2009).
- [94] W.-L. You and L. He, *J. Phys.: Condens. Matter* **27**, 205601 (2015).
- [95] W. C. Yu, S.-J. Gu, and H.-Q. Lin, [arXiv:1408.2642](https://arxiv.org/abs/1408.2642).
- [96] G. Sun, A. K. Kolezhuk, and T. Vekua, *Phys. Rev. B* **91**, 014418 (2015).
- [97] E. J. König, A. Levchenko, and N. Sedlmayr, *Phys. Rev. B* **93**, 235160 (2016).
- [98] Y.-T. Tu, I. Jang, P.-Y. Chang, and Y.-C. Tzeng, *Quantum* **7**, 960 (2023).
- [99] A. F. Albuquerque, F. Alet, C. Sire, and S. Capponi, *Phys. Rev. B* **81**, 064418 (2010).
- [100] R. Verresen, [arXiv:2301.11917](https://arxiv.org/abs/2301.11917).
- [101] Y.-W. Dai, S. Y. Cho, M. T. Batchelor, and H.-Q. Zhou, *Phys. Rev. B* **95**, 014419 (2017).
- [102] Z. Zuo, S. Yin, X. Cao, and F. Zhong, *Phys. Rev. B* **104**, 214108 (2021).
- [103] B. Žunkovič, M. Heyl, M. Knap, and A. Silva, *Phys. Rev. Lett.* **120**, 130601 (2018).
- [104] J. C. Halimeh and V. Zauner-Stauber, *Phys. Rev. B* **96**, 134427 (2017).
- [105] V. Zauner-Stauber and J. C. Halimeh, *Phys. Rev. E* **96**, 062118 (2017).
- [106] J. Lang, B. Frank, and J. C. Halimeh, *Phys. Rev. B* **97**, 174401 (2018).
- [107] J. Lang, B. Frank, and J. C. Halimeh, *Phys. Rev. Lett.* **121**, 130603 (2018).
- [108] J. C. Halimeh, M. Van Damme, V. Zauner-Stauber, and L. Vanderstraeten, *Phys. Rev. Res.* **2**, 033111 (2020).
- [109] J. C. Halimeh, N. Yegovtsev, and V. Gurarie, [arXiv:1903.03109](https://arxiv.org/abs/1903.03109).
- [110] D. Trapin, J. C. Halimeh, and M. Heyl, *Phys. Rev. B* **104**, 115159 (2021).
- [111] J. C. Halimeh, D. Trapin, M. Van Damme, and M. Heyl, *Phys. Rev. B* **104**, 075130 (2021).
- [112] M. Fishman, S. White, and E. Stoudenmire, *SciPost Phys. Codebases* **004** (2022).